# Synthesis and Properties of SMA-g-PA6 and PPO Blends via *In Situ* Active Anionic Polymerization of ε-Caprolactam, Comparing with MCPA6/PPO Blends

**Libo Du,[1,2] Guisheng Yang[1,3]**

[1]*CAS Key Laboratory of Engineering Plastics, Joint Laboratory of Polymer Science and Materials, Institute of Chemistry, Chinese Academy of Sciences, Beijing 100080, People's Republic of China*
[2]*Graduate School of Chinese Academy of Sciences, Beijing 100039, People's Republic of China*
[3]*Shanghai Genius Advanced Materials Co., Ltd, Shanghai 201109, People's Republic of China*

Received 12 February 2007; accepted 10 November 2007
DOI 10.1002/app.27818
Published online 6 March 2008 in Wiley InterScience (www.interscience.wiley.com).

**ABSTRACT:** In this work, blends of monomer casting polyamide 6 (MCPA6) and poly(phenylene oxide) (PPO) were prepared by *in situ* polymerization via the application of ε-caprolactam as a reactive solvent. Styrene-maleic anhydride (SMA) was used as both compatibilizer and macromolecular activator. With the *in situ* formed graft copolymers of SMA-g-PA6, the dispersion of PPO was much smaller, and better mechanical properties and higher heat distortion temperature were obtained. The morphologies of the blends were characterized by scanning electron microscope, and the crystallization behaviors of these blends were also studied by differential scanning calorimeter, wide angle X-ray diffraction, and polarize optical micrograph. The results showed that the main differences in crystallization behaviors and crystallographic form of PA6 between the two series blends (MCPA6/PPO and SMA-g-PA6/PPO) lie in the number and size of dispersed PA6 within the PPO rich region. Besides, the rheological properties of two series blends were also studied. SMA-g-PA6/PPO blends present higher viscosity and more elastic behavior than MCPA6/PPO blends. © 2008 Wiley Periodicals, Inc. J Appl Polym Sci 108: 3419–3429, 2008

**Key words:** anionic polymerization; compatibility; graft copolymers; polyamides; poly(phenylene oxide)

## INTRODUCTION

Polyamide 6 (PA6) is one of the most important engineering plastics, with excellent chemical resistance. However, its poor dimensional stability, low impact strength, and low heat distortion temperature (HDT) limit its application. On the other hand, poly(phenylene oxide) (PPO) exhibits high dimensional stability and good thermal properties. However, PPO also has some deficiencies such as poor solvent resistance and difficulty in processing. Therefore, the blending of polyamide and PPO may combine the advantages of both components. Because of the immiscibility, the simple melt blending generally induces deterioration in impact and tensile properties as a result of poor interfacial adhesion between the dispersed phase and the matrix that leads to rapid initiation and propagation of cracks.[1,2] Therefore, proper compatibilizer is necessary to achieve comprehensively excellent properties.

Many copolymers used as compatibilizer for the blends of PA and PPO,[3–15] such as PPO-g-MA, styrene-maleic anhydride (SMA) copolymer, styrene-*co*-acrylic acid, styrene-*co*-glycidyl methacrylate, and carboxylated polystyrene compounds have been reported. Good mechanical properties are obtained by adding PA6-grafted copolymers.[16,17] And all blends of PA and PPO were prepared through melt blending, an effective approach to disperse one polymer into the other through strong shear and reaction on the interface between different phases. In our previous work,[18–20] with dissolved PPO in caprolactam (CL), blends of PA6 and PPO were prepared by *in situ* active anionic polymerization of caprolactam. This technology has also been used to prepare PA6 blends.[21–23] However, these researches were mainly focused on the morphology and crystallization of the blends, but seldom on the effect of compatibilization on the mechanical and thermal properties.

In this article, the SMA copolymer was used as an activator to catalyze the polymerization of caprolactam. SMA-g-PA6 copolymer and SMA-g-PA6/PPO blends were synthesized. We hope that compatibility between matrix and PPO phase can be improved. Comparing with MCPA6/PPO blends, the morphology, crystallization, rheology, mechanical properties, and HDT of SMA-g-PA6/PPO blends were investigated in detail.

*Correspondence to:* G.S. Yang (ygs20002000@yahoo.com).
Contract grant sponsor: National "973" Program; contract grant number: 2003CB6156002.


© 2008 Wiley Periodicals, Inc.
WILEY InterScience® DISCOVER SOMETHING GREAT

## EXPERIMENTAL

### Materials

PPO with a $T_g$ of 218°C was obtained from GE company (Commercial Grade, BHPP 820). SMA18 ($M_w$ 1.2 × $10^5$ g/mol) is a random copolymer provided by Shanghai Research Institute of Petrochemical Technology (Shanghai, China). The weight percent (wt %) of maleic anhydride is 18. Sodium hydrate (NaOH) and toluene diisocyanate (TDI) were purchased from Shanghai Chemical Reagents Company (Shanghai, China) (Analysis Grade, P. R. China), and used without further purification.

### Blends preparation

PA6/PPO/SMA blends (SP series) preparation

ε-caprolactam was charged to a three-necked flask equipped with an air condenser, a nitrogen inlet, and a thermometer. The monomer was first exposed to vacuum at 140°C for 10 min to eliminate the absorbed water. Then PPO was added into the monomer, and dissolved at 180°C. After PPO was completely dissolved, SMA was added into the mixture, and the temperature was maintained at 180°C. At last, mixture formed a homogeneous solution. At the same time, NaOH was added into another flask containing molten caprolactam. This mixture was exposed to vacuum at 140°C for about 15 min, and caprolactam sodium (NaCL) was formed. Then the two kinds of solution were mixed and stirred fully. Several seconds later, the mixture was poured into a preheated mold in an air-circulating oven at 180°C for polymerization for 20 min. The resultant product was cooled in an air-circulating oven at 40°C. For easy control of the reaction, the MA group content in the blend was maintained at 0.037 mol/kg.

PA6/PPO blends (P series) preparation

After PPO and caprolactam solution was formed, NaCL was added into this solution. Then TDI was also added into the mixture. After fully stirring, the mixture was poured into a preheated mold. The reaction was processed in an air-circulating oven at 180°C for 20 min. The resultant product was cooled in an air-circulating oven at 40°C.

The detailed compositions of two series blends are listed in Table I. TDI was used as an activator in monomer casting polyamide 6 (MCPA6) and MCPA6/PPO blends, while SMA was used as an activator in SMA-g-PA6/PPO blends. Isocyanate could react with caprolactam to form acyl caprolactam (Fig. 1, $A_1$), while maleic anhydride groups are easy to react with NaCL to form acyl caprolactam (Fig. 1, $A_2$). The acyl caprolactam could catalyze the active anionic polymerization of ε-caprolactam, and induce PA6 chain to grow from these active dots. Finally, the backbone of SMA grafted PA6 chains, forming a comb-like copolymer. This copolymer is *in situ* formed and can be used to compatibilize PPO and PA6 phases. Figure 1 briefly presents the process of the active anionic polymerization of ε-caprolactam.

**TABLE I**
**Composition of Two Series Blends and Polymer Yield**

| Designation | PPO (g) | SMA18 (g) | CL (g) | NaOH (g) | TDI (mL) | $y$ (%) |
|---|---|---|---|---|---|---|
| MCPA6 | 0 | | 500 | 1.0 | 2.0 | 96.7 |
| P1 | 10 | | 490 | 1.0 | 2.0 | 96.1 |
| P2 | 20 | | 480 | 1.0 | 2.0 | 95.9 |
| P3 | 30 | | 470 | 1.0 | 2.0 | 96.2 |
| P4 | 40 | | 460 | 1.0 | 2.0 | 95.5 |
| P5 | 50 | | 450 | 1.0 | 2.0 | 95.1 |
| SMA-g-PA6 | 0 | 10 | 490 | 2.5 | | 96.4 |
| SP1 | 10 | 10 | 480 | 2.5 | | 95.6 |
| SP2 | 20 | 10 | 470 | 2.5 | | 95.7 |
| SP3 | 30 | 10 | 460 | 2.5 | | 95.9 |
| SP4 | 40 | 10 | 450 | 2.5 | | 94.4 |
| SP5 | 50 | 10 | 440 | 2.5 | | 95.0 |

### Characterization

Polymer yield and monomer conversion

The polymer yield was defined as the ratio of the mass of the polymerized CL to its initial mass. To measure the monomer conversion, a known amount of the reacting system after polymerization was first pressed into a thin film of about 100 μm. The monomer and catalyst residues in the film were then extracted by Soxhlet extraction for 48 h using ethanol as solvent. The film thus purified was dried in a vacuum oven at 100°C overnight and then weighed. The polymer yield, $y$, was then calculated according to the following expression:

$$y = \frac{W_p}{W_0}, \quad (1)$$

where $W_p$ and $W_0$ were the masses of the polymerized monomer and the initial monomer, respectively. The polymer yields of different products were listed in Table I.

### Fourier transform infrared spectroscopy (FTIR)

FTIR in attenuated total reflectance mode (ATR-FTIR) was carried out with a Nicolet AVATAR 360 FTIR spectrometer in the range 4000–650 $cm^{-1}$, with a resolution of 2 $cm^{-1}$.

### Rheology

The Rheometrics Mechanical Spectrometer, ARES rotational rheometer (Rheometrics), was used to measure

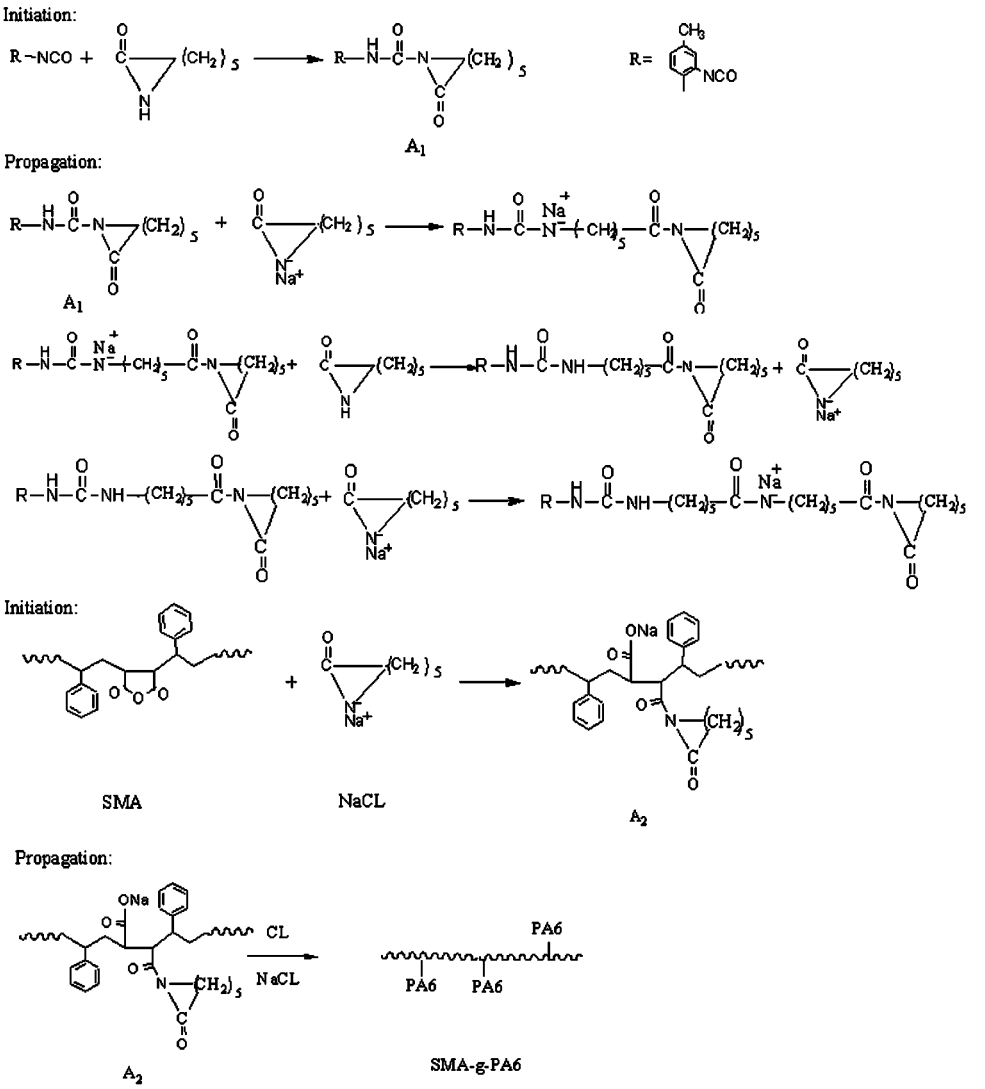


**Figure 1** Schematic representation of active anionic polymerization of ε-caprolactam with activator of TDI and SMA in different blends, respectively.

the dynamic viscosity η* and the viscoelastic modulus (G′ and G″) as function of frequency at 260°C. The experiments were carried out in the dynamic mode in parallel plate geometry at a strain of 5% and gap of 1.0 mm. The experiment was performed under dry nitrogen. Samples with a diameter of 25 mm were compression molded from the test material using a hot press machine at a temperature of 260°C. These disks were dried at 150°C under vacuum for 48 h before the measurements. The frequency was varied from 0.1 to 100 rad/s and the amplitude was kept small enough to ensure a linear viscoelastic response of the samples.

### Scanning electron microscope

The morphology was observed with a scanning electron microscope (JSM-5610LV, JEOL Co.).The samples were kept in liquid nitrogen for 10 min, and a brittle fracture was performed. The surfaces of samples were coated with gold under vacuum before observation.

### Differential scanning calorimeter

Differential scanning calorimeter (DSC) measurements were carried out on a NETZSCH DSC 200 PC calibrated by In standards. All the measurements were performed from room temperature to 250°C at a heating rate of 5°C/min under a nitrogen atmosphere. Samples were held at 250°C for 5 min to erase any previous thermal history, and then underwent subsequent cooling and heating cycles. The melt enthalpy ($\Delta H_{m2}$) in the second heating scan was used for comparison of the relative changes in crystallinity. The crystallinities of the polyamide part were determined according to the following equation:

$$X_c = \Delta H_{m2}/F\Delta H_m^*, \quad (2)$$

where $\Delta H_{m2}$ is the melting enthalpy of PA6 in the sample, $\Delta H_m^*$ is the melting enthalpy of PA6 of 100% crystallization ($\Delta H_m^* = 230$ J/g),[24] $F$ is the homopolymer weight fraction in the blend and was defined as:

$$F = \frac{W_P}{W_0 + W_a}, \quad (3)$$

where $W_a$ is the total mass of additional polymers before reaction. Moreover, $T_m$ is the melting point and $T_c$ is the maximum of the crystallization temperature. $T_{c,o}$ values, which are the initial temperature of crystallization in the cooling scan, were used for comparing the nucleating effect. The values of $\Delta T = T_{c,o} - T_c$ is relative to the growth of crystallization, so it is used for comparing the growth of crystallization of the blends.

### Polarize optical micrograph

Slices of sample of about 10 μm thick were prepared by cryogenically cut. An Olympus BH2-UMA optical microscope equipped with a Nikon CCD camera was utilized to analyze the spherulite of PA6 in the blends.

### Wide angle X-ray diffraction

Wide angle X-ray diffraction (WAXD) was performed on an X-ray diffraction analyzer (XRD, Rigaku D/Max-III, Japan) equipped with a rotating Cu anode generator system using Cu/K-αl ($\lambda$ = 1.540 Å) radiation. WAXD profiles were recorded at room temperature with diffraction angles (2θ) were from 3° to 50°. The data were accumulated for 6 s at angular intervals of 2θ = 0.1°.

### Mechanical testing

The tensile properties (ASTM D 638) of the blends were determined at room temperature with a universal testing machine (model CMT 4204, Shenzhen Xinsansi equipment Co.) with an extensometer at a crosshead speed of 50 mm/min. HDT (ASTM D 648) was determined on a heat distortion and Vicat soften temperature testing machine (model ZWK 1302, Shenzhen Xinsansi equipment Co.)

## RESULTS AND DISCUSSION

### Characterization of the graft copolymer of SMA-g-PA6

FTIR spectra of MCPA6, SMA, and SMA-g-PA6 are presented in Figure 2. The peaks at 1852 and 1774 $cm^{-1}$ are corresponding to the stretch vibration of C=O on maleic anhydride group. Although in SMA-g-PA6 spectra, these two peaks disappeared, a new peak appeared at 1738 $cm^{-1}$. This peak is corresponding to the C=O group that joins the amide group. Besides, the peak at 1637 and 1540 $cm^{-1}$ are corresponding to amide group of PA6. Thus, the existence of the graft copolymer of SMA-g-PA6 is obvious.

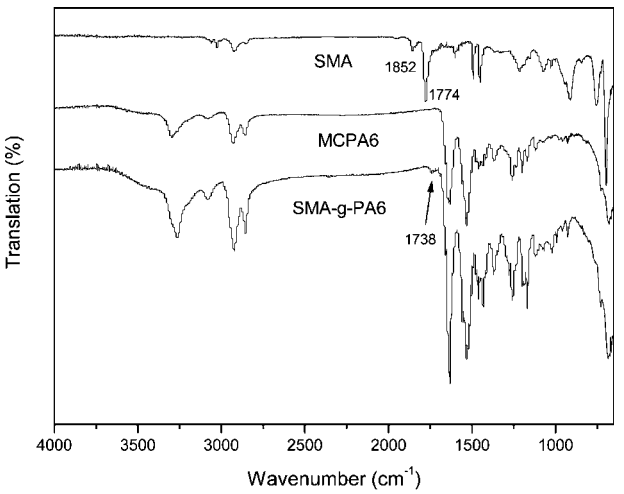


**Figure 2** FTIR spectra of MCPA6, SMA, and SMA-g-PA6.

### Morphologies of MCPA6/PPO and SMA-g-PA6/PPO blends

PPO is completely miscible with polystyrene at any proportion, so many kinds of polystyrene copolymer have been used as compatibilizer in PA/PPO blends, among which maleic anhydride and styrene random copolymer are effective ones. In this work, maleic anhydride group is also used as an activator in anionic ring-opening polymerization of caprolactam.

As seen in Figure 3, the MCPA6/PPO blends present guava-like morphologies when PPO content is above 2 wt %. This figure also shows that the PPO region extends from several micrometers to several hundred micrometers with increase of its content. In addition, both the number and size of PA6 spherules dispersed in PPO increase too. The largest phase size of PA6 inclusion is more than 10 μm. When the content of PPO is above 6 wt %, the PPO region extends too rapidly to see one whole region at the same magnification.

The detailed mechanism for formation of PA6 inclusion is described as follows. At first, PPO is dissolved in caprolactam and a homogeneous solution forms. With the advance of polymerization, more and more caprolactam is polymerized into PA6, which is immiscible with PPO, so PPO molecules aggregate to form PPO spherules. For the fast rate of active anionic polymerization, the solution solidifies only after about 2 min. Therefore, PPO molecules do

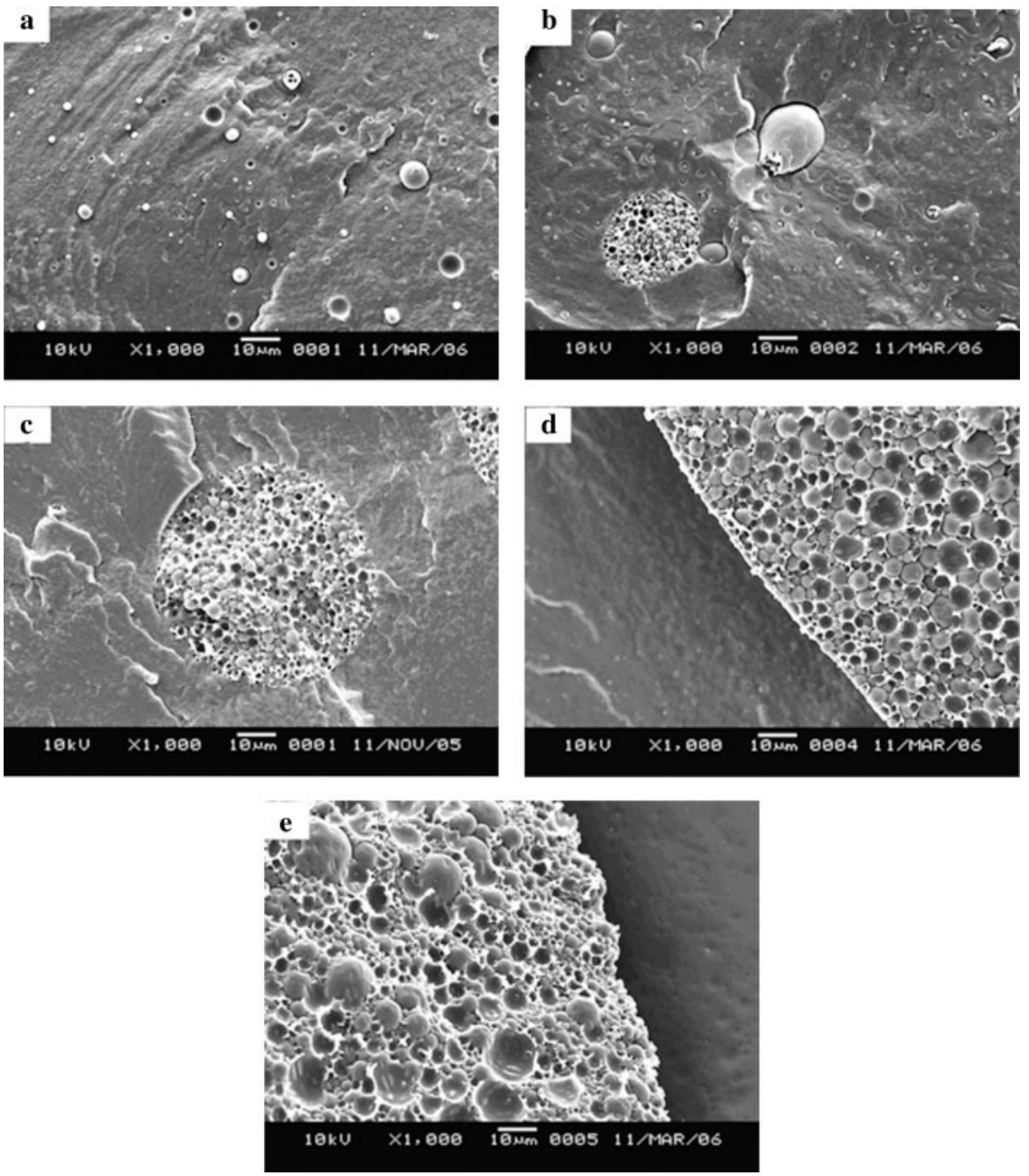


**Figure 3** Morphologies of MCPA6/PPO blends: (a) 2 wt % PPO; (b) 4 wt % PPO; (c) 6 wt % PPO; (d) 8 wt % PPO; (e) 10 wt % PPO, the magnification is 1000.

not have enough time to assemble fully. As a result, part of the monomer is included in PPO-rich region and formed the PA6 inclusion at last. Hence, larger the amount of PPO in the blend, more is the PA6 contained in PPO.

After adding SMA18 instead of TDI as activator, the morphologies of SMA-g-PA6/PPO blends (SP series blends) (Fig. 4) differ markedly from that of the MCPA6/PPO blends (P series blends). From Figure 4(a–e), the PPO-rich region becomes larger with the increasing amount of PPO, but not as rapidly as in the MCPA6/PPO blends. Moreover, the sizes of contained spherules are maintained below 2 μm. Compared with the MCPA6/PPO blends, the distribution of PPO in SMA-g-PA6/PPO blends is more uniform. When the content of PPO reaches 10 wt %, the PPO region has a tendency to form network, and the matrix is inclined to form spheres. The morphologies of the SMA-g-PA6/PPO blends are affected mainly by two factors. On the one hand, maleic anhydride group as an activator can induce monomer polymerization on it, thus, all the PA6 chains graft on the SMA backbone. This graft copolymer has larger molecular weight and long-branch chains. The entangle-

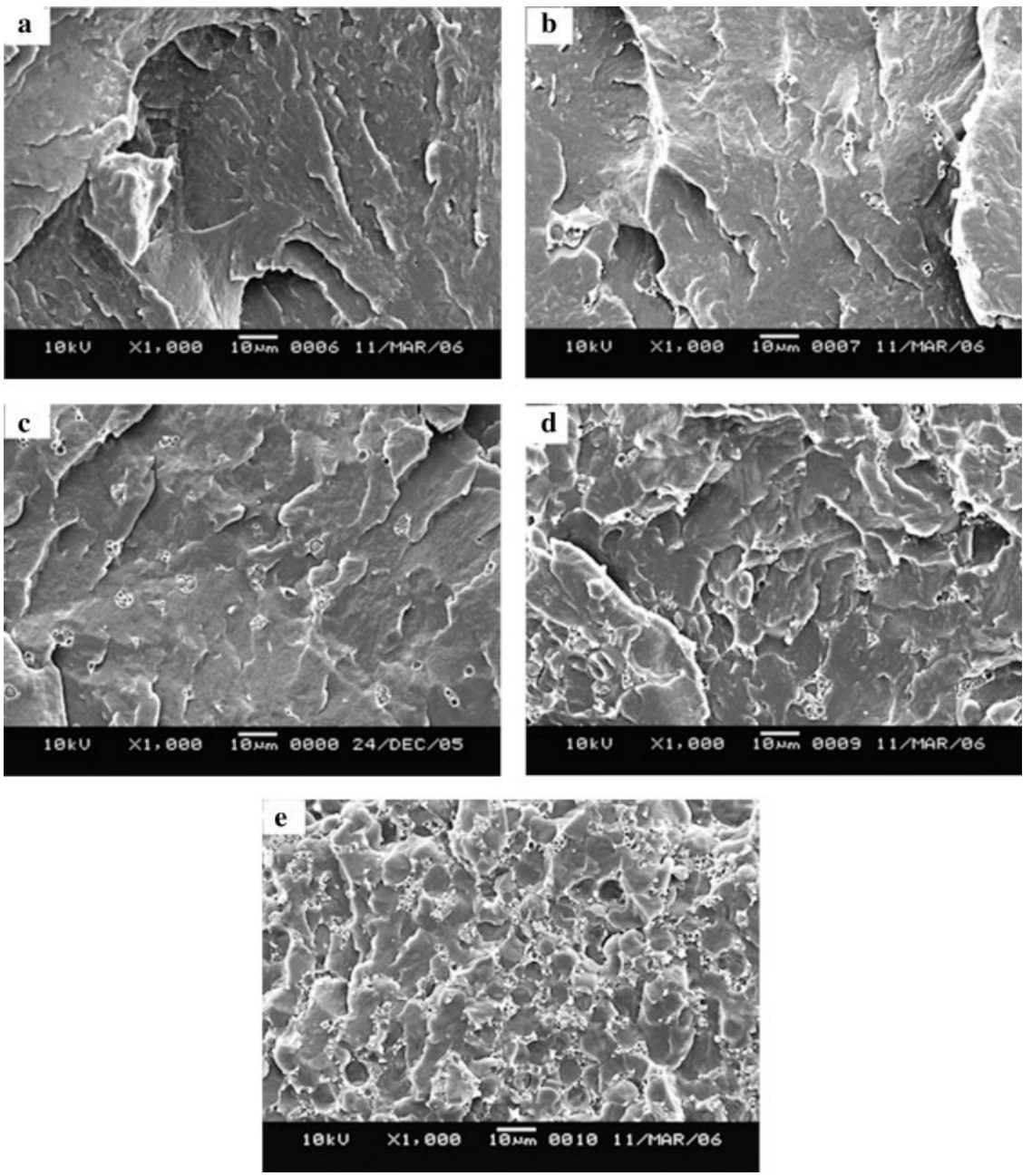


**Figure 4** Morphologies of SMA-g-PA6/PPO blends: (a) 2 wt % PPO; (b) 4 wt % PPO; (c) 6 wt % PPO; (d) 8 wt % PPO; (e) 10 wt % PPO; the magnification is 1000.

ment of branch chains prevents PPO from getting together. On the other hand, the polystyrene chain segments on SMA18 compatible with PPO[25–27] also slow the congregation of PPO molecules. Because of the fast rate of active anionic polymerization, this factor can play an important role in the terminal structure of the blend.

### Crystallization of two series blends

#### DSC

The thermal characteristics of the MCPA6/PPO and SMA-g-PA6/PPO blends are listed in Table II.

The DSC thermograms of the two series materials at cooling cycle are presented in Figure 5. As seen in Figure 5(a), $T_c$'s of MCPA6/PPO blends are obviously lower than that of neat MCPA6. From Table II, $T_{c,o}$ has the same trend as $T_c$ in MCPA6, P1, P3, and P5. In addition, the $\Delta T$ becomes larger with increasing PPO content in P series blends. This demonstrates that the existence of PPO restricts not only the nucleation but also the growth of crystals. Moreover, the enthalpy of crystallization ($\Delta H_c$) decreases with the increasing PPO amount, which also implies that the crystallization of PA6 in the MCPA6/PPO blends is suppressed by the presence of PPO. The

rapid drop of $\Delta H_c$ can be explained as follows. First, because the glass transition temperature of PPO is 218°C, higher than $T_{c,o}$ of PA6, the movement of PA6 molecules chain is confined when PPO molecules have achieved vitrification. Second, the dispersed PA6 with little size in PPO region is difficult to nucleate and crystallize perfectly. Thus, as the amount of dispersed PA6 increases, the $\Delta H_c$ of PA6 decreases. It is interesting that in case of PPO amount of 10 wt %, two peaks at 140.2°C and 177.9°C appear with $\Delta H_c$ being 5.15 and 36.13 J/g, respectively. The smaller peak is attributed to the crystallization of dispersed PA6, while the larger peak is attributed to the crystallization of matrix PA6. Why this phenomenon does not appear in P3? It is suggested that though there also exist many dispersed PA6 in the blend P3, the PPO-rich region is not large enough and the amount of dispersed PA6 is so little compared with the matrix that the crystallization of PA6 inclusion in P3 blend can not be detected by the DSC.

Figure 5(b) displays the cooling scan of SP series blends. The $T_c$ of SMA-g-PA6 is lower than that of MCPA6. This is because the molecules of SMA-g-PA6 are comb-like; the PS chain segments of the grafted molecule block the mobility of PA6 chains and prevent them from orderly arranging in crystalline lattice. Moreover, $T_{c,o}$ of SMA-g-PA6 is lower than that of MCPA6, demonstrating that the nucleation is more difficult in SMA-g-PA6. With the addition of PPO, the PS chain segments are partially miscible with PPO, while PPO is immiscible with PA6, so it is inclined to form morphology as shown in Figure 7. In this model, the grafted PA6 chains on SMA disperse around the backbone in SMA-g-PA6. With addition of PPO, the chains of PA6 are immiscible with PPO, so they incline to separate from each other. On the contrary, PS chain segments are miscible with PPO, and incline to disperse in PPO. At last, the PA6 chains mostly exist on one side. Thus, the density of PA6 chain and hydrogen bond both increase. As a result, PA6 chains are much easier to assemble in order during cooling process with less blocking. This effect of PPO leads to the rise in $T_c$ and $T_{c,o}$ of SP1, SP3, and SP5 compared with SMA-g-PA6. Besides, the values of $\Delta T$ decreases as the PPO content increases. These results demonstrate that the nucleation and growth of crystallization are both prompted by adding PPO. This deduction can also be proved from the $\Delta H_c$ of PA6 maintaining around 50 J/g in SP series blends. Compared with P5, there is only one peak in the cooling scan of SP5. It is because the dispersed PA6 in SP5 are much less than that of P5.

In the second scan of heating (Fig. 6), the two series of blends show a similar trend. With the increase in the amount of PPO, the shoulders corresponding to the melting of γ-crystals of PA6 become larger. This is in conformity with WXRD measurement. The crystallinities of MCPA6/PPO blends decrease with the increases of PPO content. Whereas,

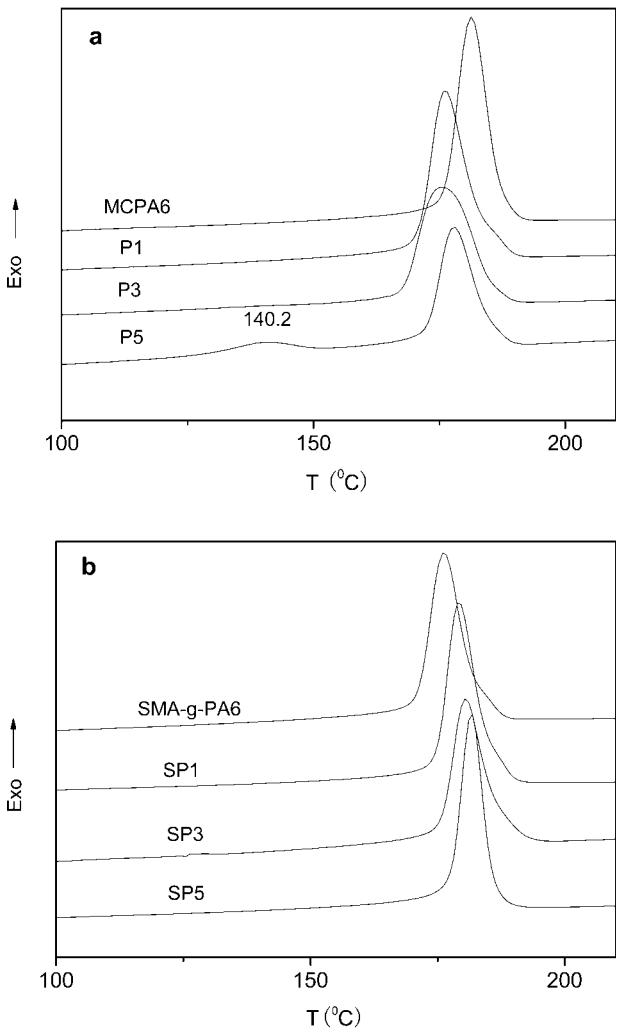


**Figure 5** DSC thermograms of the two series materials at cooling cycle: (a) neat MCPA6 and MCPA6/PPO blends; (b) SMA-g-PA6 and SMA-g-PA6/PPO blends.

**TABLE II**
**Thermal Properties of MCPA6/PPO and SMA-g-PA6/PPO Blends**

| | $T_{c,o}$ (°C) | $T_c$ (°C) | $T_{m2}$ (°C) | $\Delta T$ (°C) | $X_c$ (%) | $\Delta H_c$ (J/g) |
|---|---|---|---|---|---|---|
| MCPA6 | 187.30 | 181.35 | 220.20 | 5.95 | 26.53 | 64.87 |
| P1 | 183.67 | 176.31 | 219.62 | 7.36 | 25.68 | 60.35 |
| P3 | 185.63 | 175.58 | 219.22 | 10.05 | 25.62 | 52.31 |
| P5 | 185.06 | 177.94 | 219.93 | 7.12 | 22.75 | 36.13 |
| | 150.13 | 140.21 | | 9.92 | | 5.15 |
| SMA-g-PA6 | 182.69 | 176.21 | 217.76 | 6.48 | 21.94 | 51.14 |
| SP1 | 185.47 | 179.24 | 219.22 | 6.23 | 23.32 | 52.86 |
| SP3 | 184.25 | 180.40 | 218.63 | 6.63 | 24.86 | 48.27 |
| SP5 | 185.86 | 181.76 | 217.85 | 4.10 | 23.24 | 50.28 |

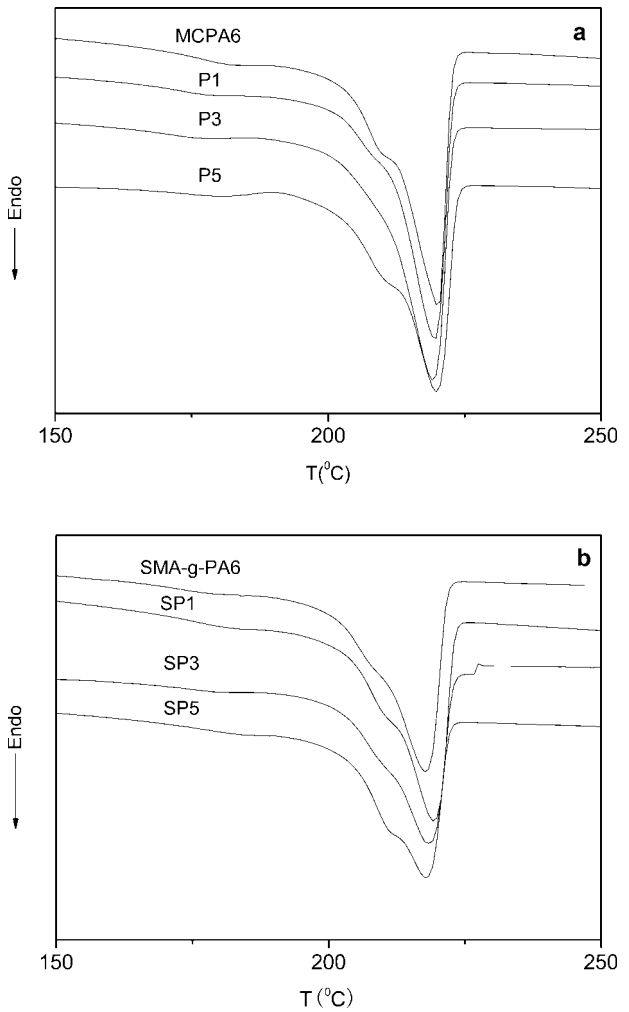


**Figure 6** DSC thermograms of the two series materials at second heating cycle: (a) neat MCPA6 and MCPA6/PPO blends; (b) SMA-g-PA6 and SMA-g-PA6/PPO blends.

the crysallinities of SMA-g-PA6/PPO blends ascend with the increase of PPO from 2 to 6 wt %, then descend when the PPO content reaches 10 wt %. The reason of ascend trends can be explained by the model in Figure 7. And the decrease of crystallinity is the result of excessive PPO that restrains the crystallization of PA6.

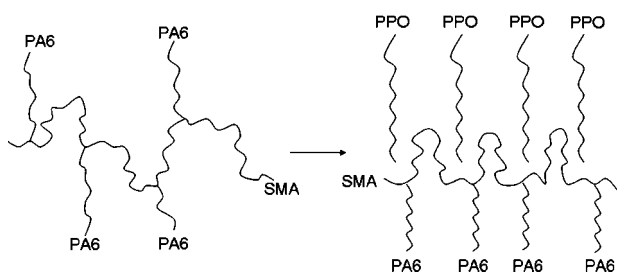


**Figure 7** Model of the arranging change of PA6 chains on SMA-g-PA6 molecule by adding PPO.

## WAXD

The WAXD spectrums of MCPA6, P5, SMA-g-PA6, and SP5 are shown in Figure 8. The cooling rate (5°C/min) during DSC measurements is faster than that of cooling at 40°C in an air-circulating oven. So, PA6 is inclined to form the stable α-crystal in the latter condition. After original samples are annealed at 150°C for 24 h, crystals become much more perfect. The monoclinic α-crystal can be identified from WAXD measurement according to the presence of pair diffraction peaks at 2θ of 20.1° {200} and 23.6° {002} + {202}. In the pure MCPA6 and SMA-g-PA6, only α-crystals appear. With addition of 10 wt % PPO, a new small peak emerges at 21.38°, corresponding to the γ-crystal of PA6. This phenomenon appear both in P5 and SP5, but the γ-crystal peak of SP5 is much smaller than that of P5. The result of

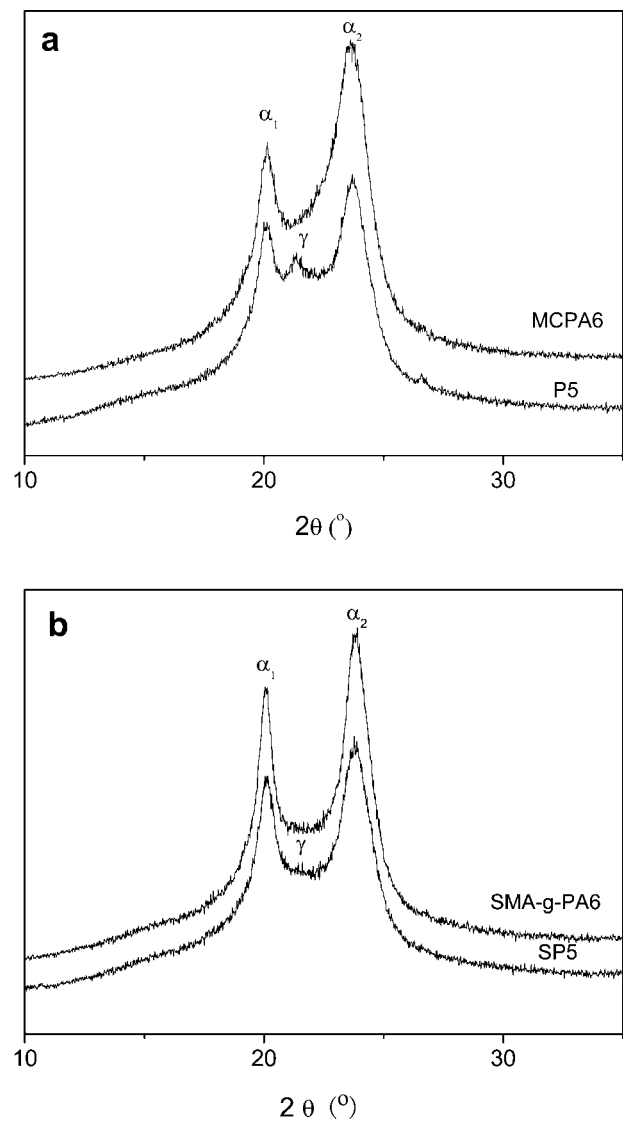


**Figure 8** WAXD spectrums of (a) MCPA6 and P5; (b) SMA-g-PA6 and SP5 after annealing at 150°C for 24 h.

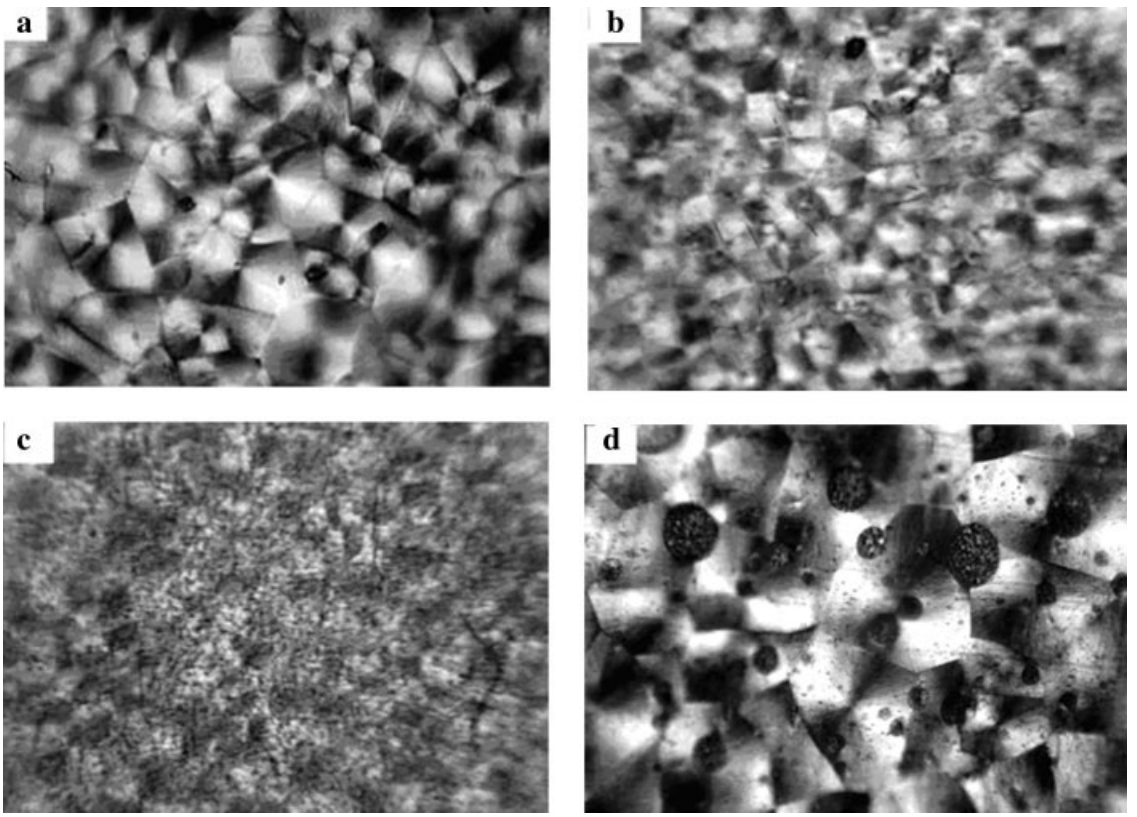


**Figure 9** Polarize optical micrograph of (a) SMA-g-PA6; (b) SP3; (c) SP5; (d) P3. The magnification is 200.

WAXD spectrums demonstrates that the contained PA6 spherules in PPO region tend to form γ-crystals due to the confinement of PPO. It has been reported in several papers that the confined PA6 phase is easy to form γ-crystal.[28,29]

## POM

The polarize optical micrograph of the SMA-g-PA6, SP3, SP5, and P3 are displayed in Figure 9. From the picture of SMA-g-PA6, SP3, SP5, it is obvious that the PA6 spherulite size decreases as the PPO content increases, which implies that PPO can prevent PA6 chains from forming spherulites. This inference is in accordance with the morphology in Figure 4(e), where the matrix is divided into smaller regions of about 5 μm by PPO-rich regions. For SP3 and P3, with the same PPO content, the sperulite size of PA6 in P3 is much larger than that in SP3. Moreover, PPO-rich regions in Figure 9(d) are very clear, while the PPO-rich regions in Figure 9(b) are present in some particles.

This demonstrates that the movement of grafted PA6 chains is confined by the backbone of SMA, and the chains are difficult to move freely to form larger spherulites. Moreover, the compatibilization of SMA leads to the finer dispersion of PPO, so the spherulites are confined much more by PPO.

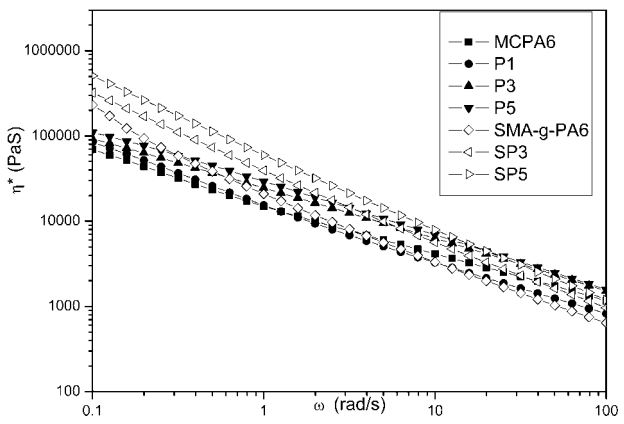


**Figure 10** Complex viscosities versus frequency curves of MCPA6, P1, P3, P5, SMA-g-PA6, SP3, SP5 blends. All experiments were carried out at 260°C.

## Rheological properties

The morphology of polymer blend is closely related to its rheology. Therefore, the rheological properties of the MCPA6/PPO blends and SMA-g-PA6/PPO blends have been studied here (Figs. 10 and 11). Figure 10 shows plots of complex viscosity (η*) as a function of frequency (ω) for the two series blends.

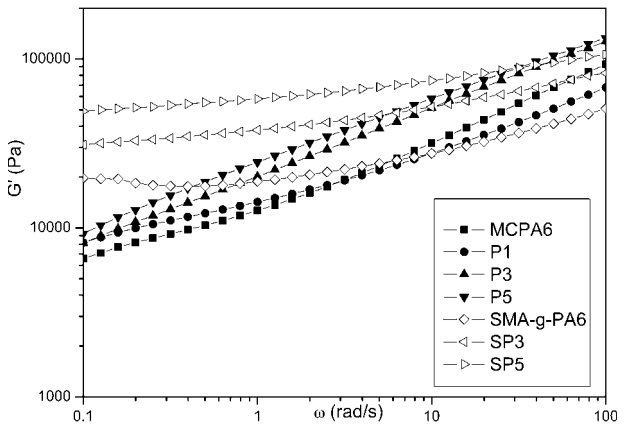


**Figure 11** Dynamic storage modules versus frequency curves of MCPA6, P1, P3, P5, SMA-g-PA6, SP3, SP5 blends. All experiments were carried out at 260°C.

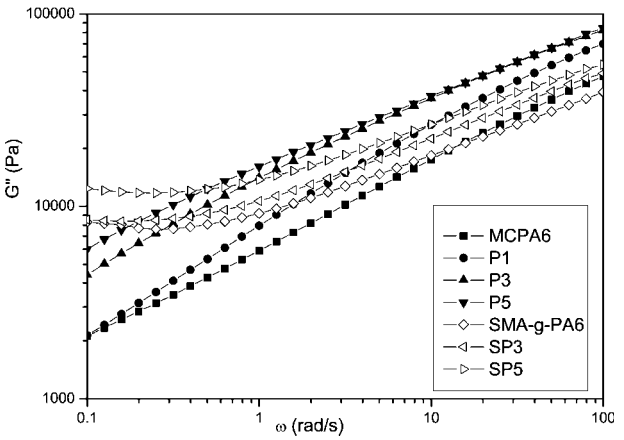


**Figure 12** Dynamic loss modules versus frequency curves of MCPA6, P1, P3, P5, SMA-g-PA6, SP3, SP5 blends. All experiments were carried out at 260°C.

A progressive increase in complex viscosity with the content of PPO can be observed over the entire frequency. This may be due to the higher melt viscosity of PPO relative to PA6.

The effect of SMA-g-PA6 on the complex viscosity can also be seen from Figure 9. With addition of SMA, the complex viscosity presents an increase at low frequency and even a slight decrease at high frequency, compared with the corresponding blends of the same PPO content. It is noted that all blends exhibit a typical shear-thinning behavior, and the shear-thinning behavior of SMA-g-PA6/PPO blends is faster than that of MCPA6/PPO blends due to the long branched chains of SMA-g-PA6. The significant enhancement of viscosity of the compatibilized blends can not only be attributed to the enhanced interfacial adhesion but also be attributed to the high molecular weight of the grafted copolymer.

The dynamic storage modulus (G′) is related to the elastic behavior of the material and may be considered as the storage energy. The dynamic loss modulus (G″) represents the dissipated energy. The dependence of G′ and G″ on the frequency measures the relative motion of all molecules in the bulk and can give important information about the flow behavior of melts.

Figures 11 and 12 show the dependence of the viscoelastic modulus on frequency for the two series blends. It is observed that both G′ (ω) and G″ (ω) of SP series is higher than that of P series at low frequency, but lower at high frequency. An apparent plateau in G′ and G″ at low frequency is observed. All these can be explained by the strong interaction existing in the SP series blends to form a quasi-network structure that results from the entanglements of SMA-g-PA6 and PPO due to their well compatiblization and high molecular weight of the grafted copolymer.

## Mechanical properties and HDT

A compatibilized polyblend, in general, has finer phase domain, greater interfacial contact area, and stronger interfacial adhesion than the corresponding uncompatibilized blend that is critical to stress transfer between phases. However, the finer domain of the blend alone does not guarantee toughness improvement. The way the compatibilizer affects the inherent properties of the constituent matrices also needs to be taken into consideration. Table III summarizes all the mechanical properties as well as heat deformation temperature.

In Table III, with the PPO content increases, both the tensile strength and elongation at break of MCPA6/PPO blends decrease, especially with PPO content higher than 8 wt %. The decrease of mechanical properties is the result of poor interfacial adhesion between PPO and PA6 phases. When PPO content is above 8 wt %, because of the formed large domains of PPO, crack is easy to develop along the

**TABLE III**
**Mechanical Properties and HDT of Two Series Blends**

| Designation | Tensile strength (MPa) | Elongation at break (%) | Heat distortion temperature at 1.82 MPa (°C) |
|---|---|---|---|
| MCPA6 | 65.7 | 84 | 57.0 |
| P1 | 59.4 | 88 | 60.7 |
| P2 | 54.5 | 60 | 65.5 |
| P3 | 50.8 | 44 | 67.5 |
| P4 | 31.3 | 14 | 72.1 |
| P5 | 21.3 | 5 | 77.0 |
| SMA-g-PA6 | 51.0 | 274 | 61.3 |
| SP1 | 52.6 | 205 | 63.7 |
| SP2 | 56.2 | 158 | 67.8 |
| SP3 | 54.8 | 84 | 73.4 |
| SP4 | 52.7 | 64 | 76.8 |
| SP5 | 54.0 | 39 | 81.6 |

interface, which leads to the deterioration of mechanical properties.

The tensile strength of SMA-g-PA6 reduces compared to MCPA6, while the elongation rises obviously. For lower crystallinity of PA6 in SMA-g-PA6, the tensile strength is much smaller than that of MCPA6. Whereas, the elongation at break increases due to the much larger molecular weight of the graft copolymer and lower crystallinity. As PPO content increases, the tensile strength maintains around 54 MPa, while elongation decreases rapidly.

HDT is a parameter reflecting the module as a function of temperature. Generally, the more rigid the molecule is, the higher the module appears. The HDTs of two series blends show the same trend, both ascend as PPO content increases. This is mainly due to the rigid PPO molecules with high $T_g$. On the other hand, SMA also has higher $T_g$ than PA6. There are two kinds of segments that confine the movement of PA6 segments in SP series blends. Whereas, only PPO in P series blends prevents the movement of PA6 segments. The poor interaction and nonuniform distribution of PPO phase in P series blends are also the factors leading to lower HDT than that of corresponding SP series blends.

## CONCLUSIONS

SMA copolymer acts as an activator in the active anionic polymerization of caprolactam. The PA6 chains graft from SMA backbone forming a comb-like copolymer. This copolymer is partially compatible with PPO molecules. Because of the compatibility between SMA-g-PA6 and PPO, the size of PPO rich phases reduces, and meanwhile, both the number and size of dispersed PA6 in PPO phase decrease too. The movement of PA6 chains on comb-like copolymer is confined, leading to the formation of smaller spherulits. In two series blends, PA6 inclusions are inclined to crystallize in γ form with high PPO content, though the γ-crystal peak in SP5 is much smaller than that in P5. Besides, a lower crystallization peak appears in P5 with 10 wt % PPO content, while this phenomenon does not appear in SP series blends and other P series blends. It depends on the number and size of inclusions.

SP series blends show higher viscosity compared with P series. At low frequency, the viscosities rise with the PPO content increasing in both two series blends. Because of the large molecule weight grafted copolymer existing in SP series blends, the storage modules and loss modules of SP series blends are less sensitive to the frequency than that of P series.

The mechanical properties of two series blends also show some difference especially at high PPO content. The SP series exhibit better tensile properties. The HDTs of SP series blends are also higher than that of P series at the same PPO content.

The authors acknowledge with gratitude the support from Shanghai Genius Advanced Material Co., Ltd.

## References

1. Chiang, C. R.; Chang, F. C. J Polym Sci Part B: Polym Phys 1998, 36, 1805.
2. Tucker, P. S.; Barlow, J. W.; Paul, D. R. Marcromolecules 1988, 21, 1678.
3. Chiang, C. R.; Chang, F. C. J Appl Polym Sci 1996, 61, 2411.
4. Ji, Y. L.; Li, W. G.; Ma, J. H.; Liang, B. R. Macromol Rapid Commun 2005, 26, 116.
5. Wang, X.; Li, H. J Appl Polym Sci 2000, 77, 24.
6. Hseih, D. T.; Peiffer, D. G. Polymer 1992, 33, 1210.
7. Strobl, G. R.; Bendler, H. T.; Kambour, R. P. Macromolecules 1986, 19, 2683.
8. Wang, L. H.; Proter, R. S. J Polym Sci Polym Phys Ed 1983, 21, 907.
9. Kambour, R. P.; Bendler, J. T.; Bopp, R. C. Macromolecules 1983, 16, 753.
10. Zroguz, A. Z.; Baysal, B. M. J Appl Polym Sci 2000, 75, 225.
11. Jo, W. H.; Ki, H. C. Polym Bull 1992, 27, 465.
12. Laverty, J. J.; Ellis, T.; Ogara, J.; Kim, S. Polym Eng Sci 1996, 36, 347.
13. The, J. W.; Rudin, A. Polym Eng Sci 1992, 32, 1678.
14. Bhatia, Q. S.; Burell, M. C.; Chera, J. J. J Appl Polym Sci 1915, 1992, 46.
15. Macroumanchia, A.; White, R. P.; Rostani, D. M. Macromolecules 1984, 17, 17.
16. Kazuhiro, M.; Yousuke, W.; Tomoyuki, I.; Teiichi, T.; Kenzo, I. Macromolecules 1996, 29, 3694.
17. Lai, Y. C. J Appl Polym Sci 1994, 54, 1289.
18. Li, Y. L.; Xie, T. X.; Yang, G. S. J Appl Polym Sci 2006, 99, 2076.
19. Li, Y. L.; Yang, G. S. Macromol Rapid Commun 2004, 25, 1714.
20. Hou, L. L.; Yang, G. S. Macromol Chem Phys 2005, 206, 1887.
21. Ji, Y. L.; Ma, J. H.; Liang, B. R. Polym Bull 2005, 54, 109.
22. Ji, Y. L.; Ma, J. H.; Liang, B. R. Mater Lett 1997, 2005, 59.
23. Ou, Y. C.; Si, M. Y.; Yu, Z. Z. J. Appl Polym Sci 1999, 73, 767.
24. Evstatiev, M.; Schultz, J. M.; Petrovich, S.; Georgiev, G.; Fakirov, S.; Friedrich, K. J Appl Polym Sci 1998, 67, 723.
25. Gan, P. P.; Paul, D. R. J Appl Polym Sci 1994, 54, 317.
26. Fried, J. R.; Hanna, G. A. Polym Eng Sci 1982, 22, 705.
27. Witteler, H.; Leiser, G.; Drosher, M. Makromol Chem Rapid Commun 1993, 14, 401.
28. Tol, R. T.; Mathot, V. V. F.; Reynaers, H.; Goderis, B.; Groeninckx, G. Polymer 2005, 46, 2966.
29. Zhang, X. H.; Liu, Y. Q.; Gao, J. M.; Huang, F.; Song, Z. H.; Wei, G. S.; Qiao, J. L. Polymer 2004, 45, 6959.